Cross-Process X-ray Inspection Strategy in Battery Cell Assembly

Steffen Masuch[1,2(✉)], Sophie Gräfnitz[2], and Klaus Dröder[1]

[1] Institute of Machine Tools and Production Technology, Technische Universität Braunschweig, Langer Kamp 19B, 38106 Braunschweig, Germany
{s.masuch,k.droeder}@tu-braunschweig.de
[2] PowerCo SE, Industriestraße Nord, 38239 Salzgitter, Germany
https://www.tu-braunschweig.de/iwf, https://www.powerco.de

Abstract. The production of lithium-ion battery cells (LIBs) for electric vehicles requires a considerable amount of energy and raw materials. Due to the increasing added value along the production chain, it is essential to recognise deviations in the intermediate products as early as possible using 100% inline measurement processes. For this reason, LIBs are inspected during cell assembly using plain radiography to qualitatively check their internal geometry. For safety-critical features, such as the anode-cathode-overhang (AC-overhang) in the composite, measuring methods are required that are not fulfilled by plain radiography. The use of computer tomography (CT) offers a solution for this demand. However, to realise a 100% CT inspection, the scan time of conventional systems and the number of applications along the cell assembly must be reduced.

This research presents an approach to overcome this limitation in the form of a cross-process X-ray inspection strategy based on a technical and economic analysis of the cell assembly. To reduce scan time and the number of X-ray applications, multiple internal features are measured in a single CT scan prior to electrolyte filling. An initial feasibility assessment of this inspection position is being investigated using a state-of-the-art metal-jet tube and photon counting detector. This provides an inspection time of 1 s, enabling detailed inspection to be combined in a time-efficient process. However, moving the CT inspection downstream would contradict the key objective of early defect detection. To overcome these challenges, an upstream vision system was developed. This vision system detects outliers immediately after the stacking process by detecting the position of the external feature separator in the electrode separator composite (ESC) without X-rays and at a much lower cost than CT. This approach aligns with the primary objective of early defect detection in the production chain through the cross-process inspection strategy.

Keywords: Inspection strategy · Battery production · X-ray inspection · Vision system · Fast CT

K. Dröder and T. Vietor (Eds.): CD 2024, Proceedings, pp. 53–66, 2025.
https://doi.org/10.1007/978-3-658-45889-8_5

1 Introduction

The production of LIBs for electric vehicles is very resource intensive. Early defect detection is therefore crucial to ensure resource efficiency. In addition to ecological and economic aspects, the properties of the intermediate product must be quantified during production to guarantee function and safety. Zero-defect production is the goal, to be achieved through the extensive use of 100% inspection processes. With the current testing strategy in LIB production, cost-intensive test equipment is used to check the quality of the product and to continuously optimise production processes. Not all desired requirements can be fulfilled in mass production, as economic aspects are weighted more heavily. This applies to the use of X-ray technology in high-throughput cell assembly. In this production stage individual mechanical parts are assembled to form a component, whereby the inspection of the internal and external geometry has a central role. Inline-capable, measuring non-destructive visual inspection can be used at various inspection points to check the external geometry. In contrast, the inspection of internal geometric features requires the use of X-rays. Compared to visual inspection technology, the line integration of X-ray technology is more complex due to the radiation protection and the acquisition costs are many times higher.

Another important factor for an inline X-ray application is the data acquisition time of the method. Plain radiography is a method for the assessment of the quality of a region of interest of the test object with a single image in less than half a second. However, the precision and accuracy of the process is in many cases insufficient due to the laws of central beam projection [1]. This is why the use of CT is mandatory for measurement tasks. In CT, several projections are combined to form a 3D reconstruction. Depending on the number of projections required, CT scans can take a considerable amount of time. For this reason, until recently they have only been used for sample testing. Manufacturers are promising dramatic reductions in the time required for a CT scan with new innovations, particularly the use of liquid metal-jet tubes [2]. As these systems have only been in use for a short time, the feasibility of an inline application for LIB hast to be evaluated.

The inspection of features with X-rays can be carried out at various inspection points in the production chain due to the principle of operation. A feature can either be inspected in the intermediate product or in the finished LIB at the end of the process chain. The selection of the position along the production chain of X-ray inspections is a complex challenge due to the interdependence of economic and technical factors. In this context, the challenges for the implementation of CT in high-throughput cell assembly are presented in this research using a manufacturing scenario. A new cross-process X-ray inspection strategy is then derived based on technical and economic factors. In this strategy, two approaches are pursued to reduce the measurement effort of CT. The first strategy is based on the inspection of critical inspection features using a fast CT scan at a later stage in production. The second is to add a vision system without X-ray after the stacking process to detect outliers in the cell assembly as early as possible.

2 X-ray Inspection Strategy in Cell Assembly

This chapter evaluates the inspection options in cell assembly, focusing on X-ray technology. For the economic analysis of LIB production, the data from the baseline manufacturing plant of [3] is used with the example of Battery 1 from the BatPaC model. With a capacity of 6 GWh, the production is classified as medium-sized, which has the advantage of providing a reference point for smaller and larger factories. The NMC622-G battery has 67 Ah and the total cost can be estimated at 113 $/kWh. In the scenario, 22 million prismatic cells are produced per year on 300 production days with 3 shifts of 8 h each. In cell assembly, the systems are designed with an overproduction of 37%. If 8 production lines are assumed, a cycle time of 6 s/cell must be realised. This process chain is analysed in more detail below in order to derive an appropriate X-ray inspection strategy.

2.1 Technical Analysis of Test Equipment and Value Stream Analysis of Process Chain

Figure 1 shows the production chain of the baseline manufacturing plant from [3] with the individual steps of cell assembly and possible inspection points with plain radiography. In addition, a qualitative Sankey diagram illustrates the material flow of the good and bad parts that arise in the production steps and are identified in the inspection processes. With plain radiography, there is a risk of good parts being classified as bad (false negatives). There is also a risk of bad parts being classified as good (false positive) [1]. In addition, Fig. 1B allocates the value stream along the process chain by specifying the material and production costs. The manufacturing costs of the product consist of material and production costs. For the final LIB 20% of the manufacturing costs are related to production costs and 80% to material costs. In this analysis, the overhead costs were allocated to the individual process costs [3]. Additionally, the factors general sales, administration, research and development, profit and warranty were not considered. The breakdown of production costs for each process step is in accordance with the cost overview in [4].

The output of electrode production is individual sheets of anode and cathodes consisting of a substrate coated on both sides with active material. Due to the complex manufacturing process and the use of cost-intensive raw materials in electrode production, 61.6% of the total manufacturing costs are already achieved in electrode production [3]. Further analysis of the value and cost increase in cell assembly assumes good material (true positives) is transferred from electrode and separator production to cell assembly. Cell assembly comprises the individual steps of stacking, contacting, housing and filling. All processes are carried out in a dry room atmosphere. Dry room operation is one of the major cost drivers in cell assembly, so the usable area of systems has a particular impact on production costs. In the first production step of cell assembly, anodes, cathodes and the separator are combined to form an ESC. The separator, which is ceramic-coated on both sides with a central polyethylene layer, is within this analysis considered as a purchased material and accounts for 15.8% of the total material costs of the finished LIB [3]. In the ESC, the separators typically exhibit a circumferential overhang to the anodes (SA-overhang) and the anodes in turn overhang the cathodes circumferentially

(AC-overhang). The SA-overhang is implemented to prevent electrical contact between the anode by the cathode. The AC-overhang is relevant to ensure full coverage of the cathode. The SA-overhang is implemented to prevent an electrical contact between the anode by the cathode to prevent lithium plating. The position of the separators and electrodes in the process can currently be checked with a visual inspection during the stacking process [5]. However, simultaneous X-ray detection of the separators and electrodes in the ESC after the stacking process can only be achieved with long CT scan times due to the very different X-ray attenuation of the respective materials. For this reason, there is still no inline test for the inspection of the SA-overhang. Furthermore, the only way to measure the AC-overhang in all four corners of the ESC is to perform a CT. According to recent publications, a conventional CT takes several minutes [6]. For this reason, a vision system during stacking combined with an additional plain radiography is currently the only option in high-throughput production for quality control.

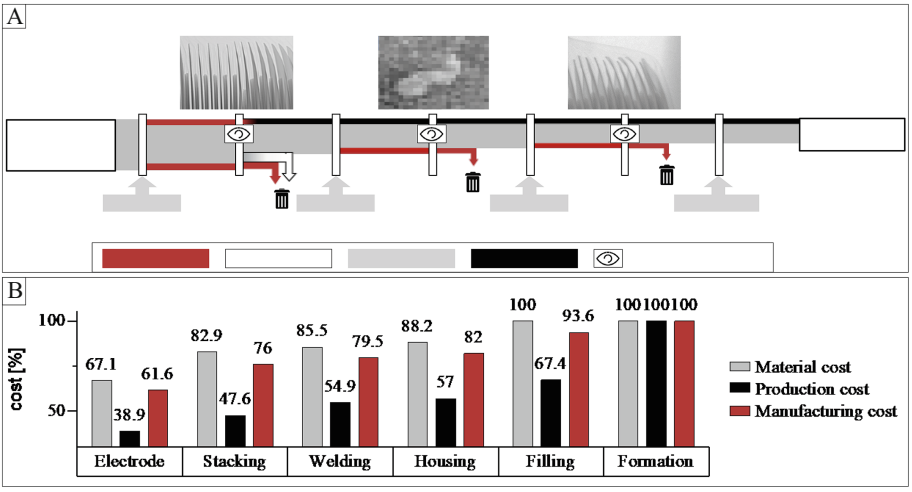

Fig. 1. **A** – Cell assembly process chain of the baseline scenario with possible options for plain radiography (RG) to test internal features of a LIB; **B** – Break-down of production, material, and manufacturing costs by individual production steps (based on [3, 4]).

In the following ultrasonic welding process, the tabs are connected to the arrester. The tabs are relatively inexpensive nickel-coated copper sheets. The requirements for the inside of the weld are the absence of pores to achieve a homogeneous current flow and a mechanically stable connection [7]. At this point, 100% defect inspection is possible using plain radiography. Plain radiography is considered highly reliable (all true positive or negative) due to its performance in defect detection, as seen in analogous tests for weld pore inspection in semiconductor manufacturing [8]. However, to measure the size and position of the pores in 3D, it is again necessary to perform a CT scan. Compared to the inspection of the AC-overhang, the requirements of the inspection without CT are fulfilled by plain radiography.

During housing, the ESC is inserted into a can. Due to the narrow tolerances between the ESC and the housing, there is an increased risk of damaging the ESC in the corner area when inserting it. It is essential to maintain a defect-free housing to prevent damage to the ESC and consequently the migration of particles and short circuits [9]. Due to the required defect detection in the corner area, tests using plain radiography fulfil the requirements. However, as with the measurement of pores in the weld seam, CT can reveal more information about the damage and the origin of defects. CT at this point would allow further analyses to be carried out over a large data set.

The final process step in the cell assembly stage is electrolyte filling, in which liquid lithium hexafluorophosphate salt, dissolved in a carbonate-based solvent system, is filled in under vacuum. At 11.8% of the manufacturing costs, the electrolyte is a comparatively expensive component of the LIB [4]. No other mechanical parts are added, and the LIB is finally sealed. Therefore, no new internal features are added at this stage.

In the next production stage, formation and ageing, the LIB is being electrochemically activated and the self-discharge rate is determined, followed by the end of line tests. In proportion, the increase in total value between cell assembly and delivery is 7.4% due to high manufacturing costs resulting from long storage times and expensive equipment [3, 4].

2.2 Cross-Process X-ray Inspection Strategy

Based on the technical and economic analysis carried out, a proposal for the use of 100% measuring X-ray inspection in high-throughput cell assembly is given below. Taking into account the factors influencing the choice of inspection technology, the inspection position and the harmonisation of the requirements of individual inspections along the entire cell assembly, the concept developed is referred to as a cross-process inspection strategy. This is illustrated below and visualised in Fig. 2.

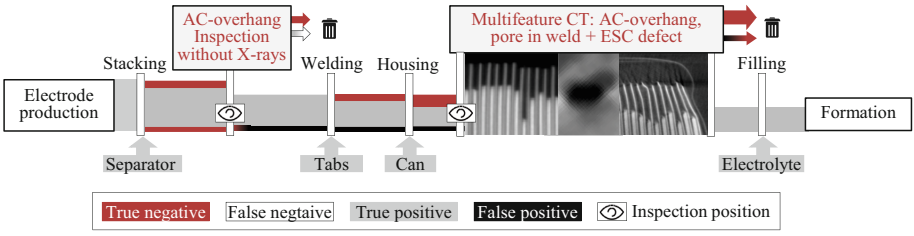

Fig. 2. Cross-process X-ray inspection strategy for implementing a multifeature CT in cell assembly.

The technical challenges of inspecting internal features were discussed. After three process steps, X-ray technology can be applied. Plain radiography can be applied after three process steps to generate individual X-ray images to visualise defects. CT scans with longer inspection times are required for measurement tasks such as determining the position of electrodes. One approach to directly reduce the measurement time is to inspect several features in one CT and accelerate the acquisition of each projection. This

inspection is called multifeature CT and has the advantage of minimising the risk of false test decisions. (false positive / negative). The idea of multifeature CT is to inspect the AC-overhang, weld defects and the position of the ESC after housing. A CT in the cell assembly should not be carried out at the end of the process chain, as the value stream analysis shows a high level of total value added during the electrolyte filling and conditioning process. It is recommended to inspect after the housing, as the increase in total value due to welding and housing is only about 6% (see Fig. 1B). This test position is also advantageous from a technical point of view, as the probability of a downstream deviation in the characteristics is estimated to be low. Despite the mentioned benefits, the concept of zero-defect production is at odds with the idea of multifeature CT at a later stage in the production chain, since rejects should be identified as early as possible. However, later inspection is possible if a robust production chain has been demonstrated or other upstream quality assurance methods can be used to achieve an early identification of good parts. For this reason, an alternative control should also be implemented after the stacking process, which identifies bad parts and must be developed in coordination with the multifeature CT. For this reason, the following chapter describes the development of a low-cost alternative inspection method without X-rays after the stacking process.

3 Ac-Overhang Inspection Without X-rays after Stacking

This section analyses whether a deviating position of the electrodes of an ESC can be identified without X-rays. To develop a new inspection process, the causes of a deviating electrode or separator position in the manufacturing process are first analysed. A new test criterion is defined based on the root cause analysis. This allows indirect control of the electrode position via the separator position. A vision system for recording the test criterion is then set up and tested.

3.1 Root Cause Analysis of Stacking and Definition of a New Test Criterion for AC-Overhang

In this example, the single sheet stacking process in the Research & Development Line of PowerCo SE is analysed. Typical position deviations of the sheets (anode A, cathode K, separator S) are shown in Fig. 3A and B. In the process, the electrodes and the separator are placed on the stacking table as individual sheets, each with a vacuum gripper. The stacking table must move to four positions to place the different sheets. The “single position error” can occur if the sheets are placed in such a way just the top sheet moves. This deposit error can occur primarily due to incorrect gripper handling. In the process itself, a vision system can be used above the stacking table after stacking to identify this typical stacking error [10]. Once a sheet has been deposited, the stack is fixed vertically by a clamping system. The position of sheets already placed in the stack may be affected during the ESC build up due to friction and transverse forces applied by the gripper, the clamping system or by the acceleration of the stack. Typical error patterns are referred to as “diagonal force errors” and can be categorised as “single step” or “multi step”. This error is not detected by the vision system above the stacking table, so a further check must be carried out at to identify this failure.

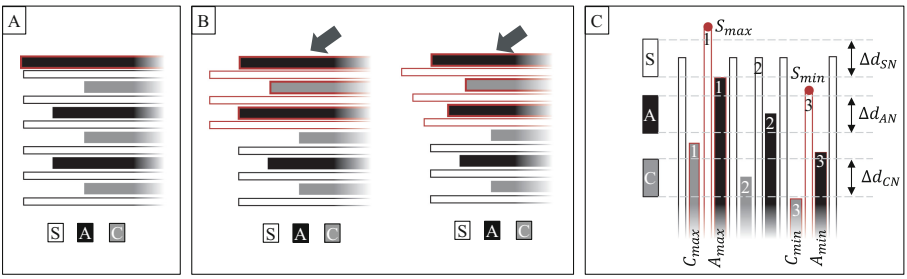

Fig. 3. **A** – Single position error; **B** – diagonal force error (left type "single step"; right "multi step"); **C** – Test criteria separator position and definition of group 1, 2, 3 of separator, anode and cathode.

For the "diagonal force error", it can be assumed that the oblique force applied to the ESC causes the adjacent sheets to move. In this scenario, or in the presence of other disturbances causing systematic displacement of adjacent sheets, the electrode position could be inferred from the position of the separators in one spatial direction. A new definition of the test criterion is shown in Fig. 3C. If there is a correlation between the separator, anode and cathode position, an outlier could be identified by defining a maximum permissible distance between separator in one spatial direction: $\Delta d_{SN} < \Delta d_S$ and $\Delta d_S = S_{max} - S_{min}$. For this outlier, it would apply that there is also a position deviation of the anodes $\Delta d_{AN} < \Delta d_A$ where $\Delta d_A = A_{max} - A_{min}$ and / or $\Delta d_{KN} < \Delta d_C$ where $\Delta d_C = C_{max} - C_{min}$ due to the large deviation of the separator position determined.

3.2 Vision System for Detection Separator Position

The separator position is an external feature which could be inspected from the lateral side using a vision system. The first step in the development of a vision system is the definition of the requirements of the object to be inspected. This data is then used to make a selection and alignment of the system components. The test object is an ESC with a total of 31 anodes (graphite), 30 cathodes (NMC622) and 61 separators. SA- and AC-overhang are 1.5 mm. The theoretical stack thickness is 11.5 mm. The sheet corners must be placed in a two-dimensional tolerance zone $\Delta d_{SN} = \Delta d_{AN} = \Delta d_{CN}$ with a width of 800 µm in one spatial direction. The smallest feature is the thickness of the separator, which is 15 µm, so according to the Shannon theorem, a digital resolution of at least 7.5 µm must be achieved [11].

The setup illustrated in Fig. 4A is developed based on these requirements. The resulting lateral image of the ESC is shown in Fig. 4B. A telecentric lens and a 10-megapixel area sensor with a pixel pitch of 3.45 µm are used for the inspection task. With the selected aperture (f-number = 10), an optical resolution of 100 lp/mm is achieved. With the magnification of the lens of 0.55 and the pixel pitch, this results in an effective resolution of 6.27 µm/pixel. The required contrast between the separator tip and the background is achieved by positioning the collimated blue illumination at an angle of 45° to the optical axis and an exposure time of 10 ms. The separators stand out as thin white lines against the black background. Manipulation of the shape of the separator can

result from contact between the anode and cathode edges. In addition, an electrostatic charge can lead to attraction between individual separator sheets. As a result of these influences, a bend to the right can be seen in all the separator sheets. It would be possible to correct the separator position by spline interpolation followed by bend correction with the length of the spline. Due to the qualitatively small differences in the magnitude of the bend, the position of the separator tip is used as the spatial position without further corrections (see Fig. 4C).

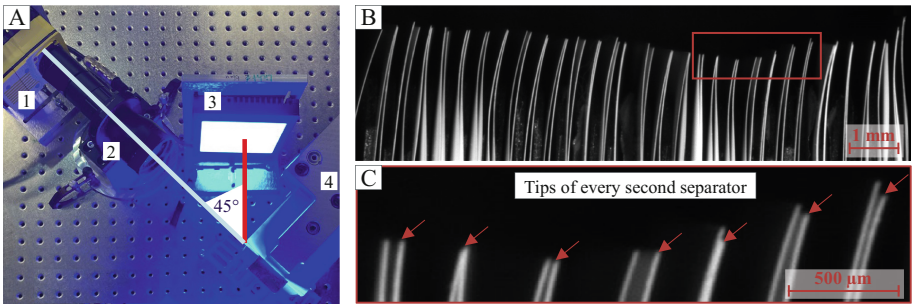

Fig. 4. **A** – Setup of vision system optical axis (white) and central beam of illumination (red), 1: camera, 2: telecentric lens, 3: collimated illuminator, 4: ESC; **B** – Resulting image of separator with high contrast of separator tips; **C** – Tips of every second separator are marked in the red section of image B.

3.3 Investigation of the Correlation Between Separator, Anode and Cathode Position

There must be a strong linear correlation in one direction between the position of the separators and the position of the electrodes in the bad ESC to use the vision system for outlier detection. For the correlation analysis, bad parts (true negative) are removed from production after the single sheet stacking process described above. No good parts are analysed because it is assumed that the position of the sheets correlate when they are correctly stacked, as the relative position differences of all sheets are small.

The bad parts are identified by CT of the corners of the ESC using the conventional system (see chapter 4, resolution 15 µm/voxel). Using this CT system, 29 ESC corners were identified which had a position distance of the long edge of the anode with $0.8\text{mm} \geq \Delta d_A \leq 3\text{mm}$ and cathodes with $0.8\text{mm} \geq \Delta d_C \leq 3\text{mm}$. . The tip position of these corners in the direction of the long edge is then recorded with the developed vision system. Finally, the tips of the separators and electrodes are labelled using the ImageJ program (version 1.52a). The pairings are numbered as shown in Fig. 3C. A labelled example images are shown in Fig. 5A. Based on the resolution of the CT and vision system, the actual position of all sheets is calculated before comparison. The main result across all pairs of anodes, cathodes and separators is shown in the diagram Fig. 5B and C. The distribution of the Pearson correlation coefficient (PCC) r across all pairs in the corner images is centred around 0.95 for the majority of the data. There are only a few

outliers, which means that this experiment demonstrated a strong correlation between the positions of adjacent separators, anodes and cathodes in one spatial direction for the stacking process investigated.

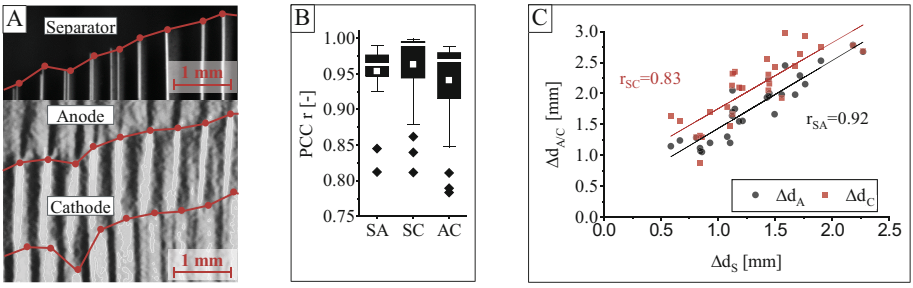

Fig. 5. **A** - Example section of labelled image data set from the vision system (top) and the CT slice (bottom); **B** - The diagram shows the PCC for the pairs of separator-anode (SA), separator-cathode (SC) and anode-cathode (AC). Over all 29 corner images the data shows a strong correlation. **C** - In the diagram, the maximum distance between the separators is plotted against the maximum distance between the anodes and cathodes of all 29 corners. The diagram visualises the linear correlation between the distances Δd_S, Δd_A and Δd_C. Compared to the difference between the anode and the separator, the difference between the cathodes is greater.

For the bad parts the criterion $\Delta d_{SN} = 0.5mm < \Delta d_S$ can serve as an indicator for an outlier, so that for anode $\Delta d_{AN} = 0.8mm < \Delta d_A$ and cathode $\Delta d_{CN} = 0.8mm < \Delta d_C$ also applies in the ESC. This is illustrated by the proof of a correlation between Δd_S, Δd_A und Δd_C which is shown in Fig. 5C. In the long term, the system must be tested further to evaluate how high the proportion of incorrect test decisions is (false positive, false negative).

4 Fast Multifeature Computed Tomography

The requirement for the realisation of a fast CT before electrolyte filling is the recording of the fastest possible projections during the rotation of the object in the X-ray beam. This requires a high tube power with a small focal spot in order to enable short exposure times for the detector [12]. As manufacturers are continuously working on this challenge, great technical progress has been made in recent years with the development of liquid metal-jet tubes and photon-counting detectors. In contrast to conventional tubes, which have a solid metal anode with air or water cooling, liquid metal-jet tubes enable considerably higher tube outputs. The increased and stable performance with a small focal spot can be achieved by the greatly improved heat dissipation through a liquid metal target made of gallium or tungsten [2]. In conventional systems, established flat-panel detectors (FPD) are also used, which convert the X-rays into an electrical signal in two steps with a scintillator layer and a photodiode. In contrast, photon-counting detectors convert X-rays in a single step, often resulting in improved image quality with higher resolution and contrast sensitivity [13]. In the following, a fast, multifeature CT with such a metal-jet

system is tested before electrolyte filling. The first part of this chapter describes the data acquisition procedure. Subsequently, CT reconstructions are presented and compared to measure several features.

4.1 Methodology

Two systems are available for perform a CT scan. The technical data and the parameters for setting the CTs are shown in Table 1. Details on the components can be found in the manufacturers' data sheets. As defined in the introduction, system 1 is referred to as a conventional system, as a closed microfocus tube (max. Power 39 W) and a FPD are installed. System 2 is defined by the use of a liquid metal beam tube (max. Power 1000 W) and a photon counting detector. The first step is to set the placement of the object and the required magnification. The test object is an ESC housed in pouch foil without electrolyte, which is shown in Fig. 6. The ESC has the same characteristics as described in Chapter 3. The results of the pouch cell are assumed to be applicable to a prismatic cell due to the relatively low X-ray absorption of the aluminium housing material compared to the ESC material. The inspection area is selected for the analysis as this is where the features to be inspected are located. An object is chosen which has all production defects to evaluate the visualisation capability in the different CT scans. For all CT scans, the object is positioned identically in the X-ray beam with the central beam between the anodes and cathodes in the corner area and the electrode edges mirror-symmetrical to the axis of rotation.

As mentioned in Sect. 2.1, the required CT scan times of less than 6 s cannot be achieved with the conventional system. For this reason, the scan with the conventional system should be of high quality and not as fast as possible. The reconstruction data is used as a comparison data set. The combination of exposure time, acceleration voltage and current is set to maximise the grey scale spectrum. A focal spot of 16.5 µm at 130 kV and 0.1 mA is used for acqusition. A stepwise exposure is performed with 720 projections and an exposure time of 200 ms. The waiting time between projections is 1 s to reduce the influence of vibrations during image acquisition. The time required to acquire the projections is 144 s. The total CT scan time, including waiting time and excluding reconstruction, is 864 s.

With the metal-jet system, two CT scans are performed to acquire data as quickly as possible. To evaluate the dependence of the quality of the CT reconstruction on the acquisition speed, two fast CT scans are performed with a total scan time of 10 s (scan 2) and 1 s (scan 3). The reconstruction time is not included in this study. In both scans, 1000 projections are acquired at 160 kV, a focal spot size of 30 µm and 4.4 mA. Scan 3 uses the detector's minimum exposure time of 1 ms. The reconstructions of all the scans are carried out with a filtered back projection and have a resolution of 20 µm/voxel. The reconstructions are aligned equally, and three slices are compared for all defect cases, which can also be seen in Fig. 6.

4.2 Results and Discussion

The evaluation of fast CT with the metal-jet system is based on a qualitative comparison of the visibility of the features and various comparative measurements with conventional

Table 1 Overview of system and CT parameters.

Parameter	Conventional System	Metal-jet System	
Tube	Hamamatsu L9181–06	Excillum MetalJet E1 + Dectris Eiger 4M	
Detector	Rad-icon 3030		
Scan	1	2	3
Goal	High quality CT	Fast CT	Fast CT
Scan time	864 s	10 s	1 s
Power	13 W	700 W	700 W
Spot size	16.5 µm	30 µm	30 µm
Voxel size	20 µm	20 µm	20 µm
Exposure time	200 ms	10 ms	1 ms
Projections	720	1000	1000

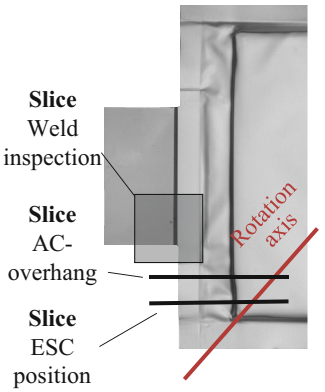

Fig. 6. Image of the test object and inspection position of slices

CT. Figure 7 shows the different raw slices of scans 1, 2 and 3. The AC-overhang (Fig. 7A), the weld seam quality (Fig. 7B) and the position of the ESC in the pouch foil (Fig. 7C) be evaluated in the slices. Basically, there is a lower signal-to-noise ratio in the fast CT scan. However, the features can still be easily identified in all scans in the manual evaluation. This is particularly evident in the qualitative analysis of the images. The position of the electrode, the weld pore, the cut in the arrester tab and the bent anode tips in the edge area can be identified in each dataset.

When the AC-overhang in the images in Fig. 7A is evaluated quantitatively using ImageJ software, it becomes clear that there are slight deviations in the position and characteristics of the features between the slices. The manual comparison measurements with three repetitions exhibit an increased difference of the mean value between the scans of the two systems. The main influencing factors are assumed to be the deviations in the

beam hardening artifacts in the anode tip area in the slices of the conventional system and a deviation in slice position due to a different alignment of the reconstructions. In contrast, the measurement deviations between scans 2 and 3 are low. In addition, the standard deviation of the manual repeat measurements is small for all measurements. Furthermore, the setting of a static threshold filter in Fig. 7C shows that an automated evaluation of all slices could be possible, since path tracking for the anodes is possible.

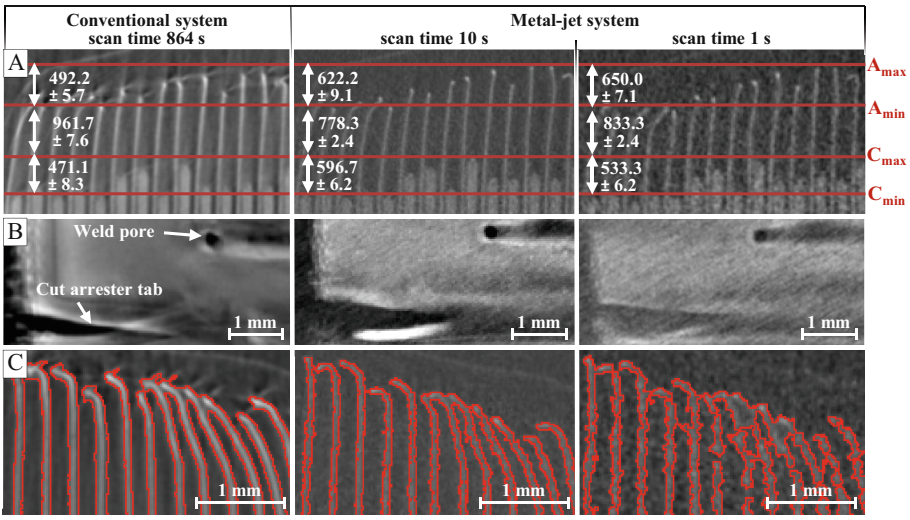

Fig. 7. **A** – Comparison of AC-overhang measurement; **B** – Slice of weld defects (cut in arrester tab and weld pore); **C** – Visualisation of anode tracing for detect bended tips

The comparison has shown that with a metal-jet system, the acquisition time of the projections for a multifeature CT can be reduced by using a liquid metal-jet tube and a photon-counting detector. Even in the shortest scan, which takes only 1 s, all inspection features can be identified. Further tests must investigate whether the required precision and accuracy can be achieved with this fast CT. The initial results show that this system can be used in the future to implement a 100% multi-feature CT inspection with the proposed cross-process inspection strategy in LIB mass production.

5 Conlusion and Outlook

In this research, a technical and economic analysis was carried out to derive a cross-process inspection strategy. The strategy replaces the multiple use of plain radiography with one application of 100% CT scan of internal features of a LIB in cell assembly. The prioritised inspection position before electrolyte filling is identified as advantageous, as all relevant inner features can already be inspected here and the economic loss between the stacking process and electrolyte filling due to the processing of bad parts is low at 6% of the manufacturing costs. Despite the advantages of using multifeature CT, two

challenges for the feasibility of this concept need to be analysed. Firstly, the cross-process strategy must ensure a low proportion of defective parts that are processed after the stacking phase. Therefore, at this stage, a cost-effective additional inspection without X-ray systems must be developed to identify outliers. These requirements are met by the vision system investigated in Chapter 3. As an alternative inspection technique, it was found that the position of the separators can be used to infer misaligned electrode positions due to the high correlation between adjacent sheets in an ESC. Secondly, conventional CTs are unable to achieve the inspection times required for 100% inspection in high throughput cell assembly. The investigation of a fast CT in Chapter 4 provides an initial benchmark. Using a liquid metal-jet tube and a photon counting detector, a fast CT scan was performed to measure AC-overhang, detect weld defects and damages of the ESC.

Further investigations must initially focus on the testing and optimisation of the vision system and the fast CT. When used in mass production, it is very important for both systems that the image data can be analysed automatically. Above all, when implementing fast CT, not only the acquisition times of the projections must be considered, but also the downstream reconstruction times up to the final inspection decision. Due to the amount of data generated, task-specific and time-optimised algorithms must be developed. In the future, the intelligent networking of the individual tests will lead to further innovations in a cross-process inspection strategy in LIB production. The developed cross-process inspection strategy can provide a crucial basis for implementing further approaches to increase efficiency in the use of cost-intensive measuring equipment.

References

1. S. Masuch, P. Gümbel, N. Kaden, and K. Dröder, “Applications and Development of X-ray Inspection Techniques in Battery Cell Production,” *Processes*, vol. 11, no. 1, p. 10, 2023.
2. A. Adibhatla, P. Takman, E. Espes, and U. Lundstrom, “X-ray sources for high throughput and extreme resolutions using liquid MetalJet technology and Tungsten targets (Conference Presentation),” in *Advances in Laboratory-based X-Ray Sources, Optics, and Applications VII*, 2019.
3. P. A. Nelson, S. Ahmed, K. G. Gallagher, and D. W. Dees, “Modeling the Performance and Cost of Lithium-Ion Batteries for Electric-Drive Vehicles”, *Third Edition*, 2019.
4. Y. Liu, R. Zhang, J. Wang, and Y. Wang, “Current and future lithium-ion battery manufacturing,” *iScience*, vol. 24, no. 4, p. 102332, 2021.
5. R. Leithoff, A. Fröhlich, and K. Dröder, “Investigation of the Influence of Deposition Accuracy of Electrodes on the Electrochemical Properties of Lithium-Ion Batteries,” *Energy Technol.*, vol. 8, no. 2, p. 1900129, 2019.
6. Niedermeier, J., Kopp, A., Schmidt, J., Schmidt, P., Bernthaler, T., & Schneider, G., Ed., “Metrologische Computertomografie zur seriennahen Anwendung an großformatigen Batteriezellen zur Qualitäts- und Funktionsbewertung,“ *DGZfP Jahrestagung*, 2018.
7. E. Rohkohl, M. Kraken, M. Schönemann, A. Breuer, and C. Herrmann, “How to characterize a NDT method for weld inspection in battery cell manufacturing using deep learning,” *Int J Adv Manuf Technol*, vol. 119, 7-8, pp. 4829–4843, 2022.
8. T. Tyystjärvi, I. Virkkunen, P. Fridolf, A. Rosell, and Z. Barsoum, “Automated defect detection in digital radiography of aerospace welds using deep learning,” *Weld World*, vol. 66, no. 4, pp. 643–671, 2022.

9. G. Qian et al., “The role of structural defects in commercial lithium-ion batteries,” *Cell Reports Physical Science*, vol. 2, no. 9, p. 100554, 2021.
10. S. Michaelis, J. Schütrumpf, J. Zienow, and A. Persichetti, “Battery Production Equipment 2030: Roadmap,” 2023.
11. F. L. Luo, H. Ye, and M. H. Rashid, *Digital power electronics and applications*. London: Elsevier Academic, 2005.
12. E. A. Zwanenburg, M. A. Williams, and J. M. Warnett, “Review of high-speed imaging with lab-based x-ray computed tomography,” *Meas. Sci. Technol.*, vol. 33, no. 1, p. 12003, 2022.
13. T. Flohr, M. Petersilka, A. Henning, S. Ulzheimer, J. Ferda, and B. Schmidt, “Photon-counting CT review,” *Phys Med.*, 79:126-136, 2020.